



Transport properties and lithium insertion study in the p-type semi-conductors AgCuO_2 and $\text{AgCu}_{0.5}\text{Mn}_{0.5}\text{O}_2$

F. Sauvage^{a,*}, D. Muñoz-Rojas^{b,*}, K.R. Poeppelmeier^a, N. Casañ-Pastor^b

^a Department of Chemistry and Materials Research Center, Northwestern University, Evanston, IL 60208-3113, USA

^b Instituto de Ciencia de Materiales de Barcelona, CSIC, Campus UAB, 08193 Bellaterra, Barcelona, Spain

ARTICLE INFO

Article history:

Received 30 July 2008

Received in revised form

10 October 2008

Accepted 12 October 2008

Available online 18 November 2008

Keywords:

Lithium batteries

Delafossite

p-Type semi-conductors

In situ XRD

Silver–copper mixed oxides

ABSTRACT

The transport properties and lithium insertion mechanism into the first mixed valence silver–copper oxide AgCuO_2 and the B-site mixed magnetic delafossite $\text{AgCu}_{0.5}\text{Mn}_{0.5}\text{O}_2$ were investigated by means of four probes DC measurements combined with thermopower measurements and in situ XRD investigations. AgCuO_2 and $\text{AgCu}_{0.5}\text{Mn}_{0.5}\text{O}_2$ display p-type conductivity with Seebeck coefficient of $Q = +2.46$ and $+78.83 \mu\text{V/K}$ and conductivity values of $\sigma = 3.2 \times 10^{-1}$ and $1.8 \times 10^{-4} \text{ S/cm}$, respectively. The high conductivity together with the low Seebeck coefficient of AgCuO_2 is explained as a result of the mixed valence state between Ag and Cu sites. The electrochemically assisted lithium insertion into AgCuO_2 shows a solid solution domain between $x = 0$ and 0.8Li^+ followed by a plateau nearby 1.7 V (vs. Li^+/Li) entailing the reduction of silver to silver metal accordingly to a displacement reaction. During the solid solution, a rapid structure amorphization was observed. The delafossite $\text{AgCu}_{0.5}\text{Mn}_{0.5}\text{O}_2$ also exhibits Li^+/Ag^+ displacement reaction in a comparable potential range than AgCuO_2 ; however, with a prior narrow solid solution domain and a less rapid amorphization process. AgCuO_2 and $\text{AgCu}_{0.5}\text{Mn}_{0.5}\text{O}_2$ provide a discharge gravimetric capacity of 265 and 230 mAh/g above 1.5 V (vs. Li^+/Li), respectively, with no evidence of a new defined phases.

© 2008 Elsevier Inc. All rights reserved.

1. Introduction

Superconducting materials with high critical temperature (high- T_c) have been subjected to a considerable amount of work in materials science and physics. High- T_c cuprates typically contain square planar arrangement of copper coordinated by four in-plane oxygen. This provides efficient bonding overlap between Cu $d_{x^2-y^2}$ and O p_x and p_y orbitals. This distinctive criterion, valid until the very recent discover of superconductivity in quaternary oxypnictides ($\text{LaO}_{1-x}\text{F}_x\text{FeAs}$ [1], LaOFeP [2,3] or LaONiP [4]), has yielded to numerous cuprate structures studied in-depth with their electronic structures (YBCO, LSCO, LBCO or La_2CuO_4 etc.). Among them, the highest T_c values have been found in mercury phases that show linear Hg–O coordinating copper layers [5]. The well-known compounds ACuO_2 , where $A = \text{Li}_2$ or Na, have also received particular attention owing to their O–Cu–O bonding which offers some similarities to the aforementioned high- T_c 's [6]. Interestingly, electrochemical investigations in Li_2CuO_2 and NaCuO_2 led to motivating new materials, namely, $\text{Li}_{1.5}\text{CuO}_2$, LiCuO_2 , NaLiCuO_2 and $\text{Li}_{0.5}\text{CuO}_2$; approach which open novel

directions for the synthesis of new mixed copper valence phases, new structures and hence would prospect new physical properties [7,8]. Recently, such a strategy has been applied to silver–copper mixed oxides allowing the synthesis of the new silver oxocuprate AgCuO_2 by electrochemically oxidizing $\text{Ag}_2\text{Cu}_2\text{O}_3$ or by using ozone as chemical oxidant [9,10].

Apart from fundamental interest, silver-based materials, for example silver delafossites ($A^{\text{I}}B^{\text{III}}\text{O}_2$) received a particular attention as they offer wider optical bandgap than the related copper delafossites to form potentially new p-type transparent conducting oxides (TCO) [11]. Solid ionic conductors [12], thermoelectrics [13], potentiometric ion sensors [14] or batteries [15] are other applications where silver-containing structures have yielded improvements. From an electrochemical point of view, the silver ion Ag^+ can be reduced to silver metal at relatively high potential (c.a. $>3.0 \text{ V}$ vs. Li^+/Li) which makes this class of materials attractive as positive electrode in lithium batteries. On the other hand, the silver metal also holds the particularity to alloy with lithium ions below 0.2 V (vs. Li^+/Li). This electrochemical reaction provides as high as 1300 mAh/g gravimetric capacity as compared to 372 mAh/g for graphite [16,17]. The reduction from Ag^+ to Ag in a crystalline structure proceeds according to a displacement reaction driven by the inserted cation in the host framework (e.g. Li^+ for lithium batteries). Impressive silver dendrites exiting the particles can result from this reduction [18]. However, within the

* Corresponding authors.

E-mail addresses: frederic.sauvage@u-picardie.fr (F. Sauvage), davidmunozrojas@gmail.com (D. Muñoz-Rojas).

exception of a very few examples, this type of insertion reaction is in general not reversible. Silver vanadium oxide $\text{Ag}_2\text{V}_4\text{O}_{11}$ (ε -SVO), the cathode material in an implantable cardioverter defibrillator (ICD) device, combines at once high chemical and electrochemical stability [15], and high discharge rate capability, owing to its good $e^-/\text{Li}^+-\text{Ag}^+$ transport properties ($\sigma_{e^-} \sim 10^{-2}-10^{-3}$ S/cm and $D_{(\text{Li}^+)} \sim 10^{-8}$ cm²/s) [19–22]. To improve on SVO, compounds exhibiting a higher Ag/*M* ratio (*M* = transition metal), which would increase the battery power delivered, such as the dense silver oxyfluoride materials like $\text{Ag}_4\text{V}_2\text{O}_6\text{F}_2$ (SVOF) [18,23] or Ag_3MoOF_5 (SMOF) [24], represents potentially new cathode materials for the next generation of ICD batteries. Within this context, we report in this work preliminary result on the transport properties of the silver oxo-cuprate AgCuO_2 and the new *B*-site mixed delafossite $\text{AgCu}_{0.5}\text{Mn}_{0.5}\text{O}_2$, which have been synthesized [25], combined with an in-depth survey of their electrochemical properties versus lithium. The electrode performance for both materials will be described. A particular emphasis has been placed to gain a better insight on the lithium insertion mechanism by means of in situ PXRD during the cathodes discharge and to identify whether any new compound be electrochemically synthesized from AgCuO_2 or $\text{AgCu}_{0.5}\text{Mn}_{0.5}\text{O}_2$ similarly to the $\text{LiCuO}_2/\text{Li}^+$ system [8].

2. Experimental

2.1. AgCuO_2 and $\text{AgCu}_{0.5}\text{Mn}_{0.5}\text{O}_2$ synthetic procedures

AgCuO_2 was synthesized by electrochemical oxidation of $\text{Ag}_2\text{Cu}_2\text{O}_3$ (reported as $\text{Ag}_2\text{Cu}_2\text{O}_4$ in Ref. [9]). For the synthesis of $\text{Ag}_2\text{Cu}_2\text{O}_3$, equimolar amounts (3.2 mmol) of $\text{CuNO}_3 \cdot 3\text{H}_2\text{O}$ (Merck, p.a. 99.5%) and AgNO_3 (Panreac, p.a., 99.98%) were dissolved in 2 mL of distilled water, and the solution was then poured into 4 mL of a 3 M NaOH solution while stirring vigorously [26–28]. The resulted precipitate was kept in suspension during 12 h with continuous stirring before being recovered by vacuum filtration, washed with water, then dried at 50 °C.

The electrochemical oxidation of $\text{Ag}_2\text{Cu}_2\text{O}_3$ was performed in alkaline media using a stirred suspension of $\text{Ag}_2\text{Cu}_2\text{O}_3$ in a 1 M NaOH solution [9]. A 1 cm² platinum foil was used as working electrode and two platinum wires (1 mm diameter) were used as pseudo-reference and counter electrodes. The latter was placed in a separate half cell, which was connected to the main cell by a glass fritted membrane to avoid direct contact with the suspension. The experiments were controlled using a McPile II, BioLogic Science Instruments Galvanostat-/Potentiostat.

The *B*-site mixed Delafossite $\text{AgCu}_{0.5}\text{Mn}_{0.5}\text{O}_2$ was synthesized using 0.10 g of AgO (Aldrich), 0.08 g of CuSO_4 (Probus) and 0.09 g of KMnO_4 (Panreac) placed in 12 ml distilled water and stirred vigorously for 40 min [25]. Afterwards, 0.93 g of NaOH were added to the suspension and stirred for 1 min. The suspension was then transferred in a 23 ml TeflonTM-lined autoclave and heated at 112 °C for 15 h. After cooling, the obtained precipitate was filtered, washed and dried at 50 °C.

2.2. Physical characterization

X-ray powder diffraction data were collected using a Rigaku X-ray powder diffractometer “Rotaflex” Ru-200B, with CuK_α radiation. Profile fitting was performed with the FullProf program [29,30] using the Thompson, Cox and Hastings Pseudo-Voigt profile function [31].

In situ X-ray diffraction (XRD) patterns were collected in a ($\theta/2\theta$) configuration using a Bruker D8 diffractometer with CuK_α

radiation ($\lambda = 0.15418$ nm). For this, a homemade electrochemical cell capped by a beryllium window functioning as the positive current collector was utilized. The cells, controlled by a Mac Pile galvanostat system, were slowly discharged at a *D/20* rate while XRD patterns were recorded.

Particle size and morphology were investigated using a Philips XL-30 Field-Emission Gun (FEG) scanning electron microscope.

Transport measurements were carried out on ~60–65% dense pellets, which were compacted and shaped by carefully pressing the particles to 4 ton/cm² using a uni-axial press and a 8 mm diameter die. This pressure was maintained at least 30 min before recovering the pellet. Room temperature DC electrical conductivity was measured by a standard four-probe Pt device (Cascade Microtech, Beaverton, OR). Conductivity values reported correspond to an average value obtained from repeating measurements on different pellet locations. Assuming continuous interconnected porosity, correction from porosity was taken into consideration by applying the Bruggeman symmetric medium equation as described by McLachlan et al. [32]:

$$\sigma_{\text{experimental}} = \sigma_{\text{real}} \left(1 - \frac{3}{2}f\right)$$

where *f* is the volume fraction of porosity. Room temperature thermopower measurements were carried out by sandwiching the pellet between a heat source and a cold sink with gold foil electrodes and welded thermocouples. Thermovoltages ΔV and temperature gradient ΔT were monitored during the decay of a short heat pulse to 100 °C from which the Seebeck coefficient was extracted after correction from the platinum reference thermopower (for $\Delta T < 20$ K). Assuming a small polaronic-type conduction in $\text{AgCu}_{0.5}\text{Mn}_{0.5}\text{O}_2$, the thermopower value was converted to electron concentration using the following formalism [33,34]:

$$Q = -\frac{k_B}{e} \ln\left(\frac{\beta(1-c)}{c}\right)$$

where k_B is Boltzmann's constant, *e* the electron charge, the spin degeneracy factor (β) is typically 2, and *c* is the fraction of sites occupied by electrons, such that the electron concentration is given by *c* times *N*, *N* being the concentration of atomic sites. The Ag site density in $\text{AgCu}_{0.5}\text{Mn}_{0.5}\text{O}_2$ is c.a. 2.104×10^{22} sites cm⁻³.

3. Results and discussion

3.1. Crystal structure description and particles morphology of AgCuO_2 and $\text{AgCu}_{0.5}\text{Mn}_{0.5}\text{O}_2$

The crystal structure of AgCuO_2 can be described as alternating layers along [001] consisting of rectangular planar CuO_4 units linked to distorted AgO_6 octahedra through edge-sharing (Fig. 1a). The silver conduction pathway is bi-dimensional within the (110) planes. Although XRD and neutron studies were initially interpreted as though AgCuO_2 structure was related to that of AgO (with linear O–Ag–O bonds between the CuO_4 layers) [35], in-depth investigation by XAS to probe the local structure of AgCuO_2 suggested a more complicated environment for the silver since this latter would adopt a 2+4 coordination forming a highly distorted octahedron [36].

Following the procedure described in the experimental part, the product is single phase and the refined lattice cell parameters of AgCuO_2 are $a = 6.0620(4)$ Å, $b = 2.8020(2)$ Å, $c = 5.8594(4)$ Å, and $\beta = 107.83(9)^\circ$ (Fig. 2a). The particles size is lower than 500 nm and tends to have platelet-like morphology (Fig. 2a in inset).

Although chemically closely related, $\text{AgCu}_{0.5}\text{Mn}_{0.5}\text{O}_2$ exhibits 3*R*-delafossite structure with *R*-3*m* space group [10]. Ag^+ is linearly coordinated with two oxygen along [001] (Fig. 1b). Cu^{II}

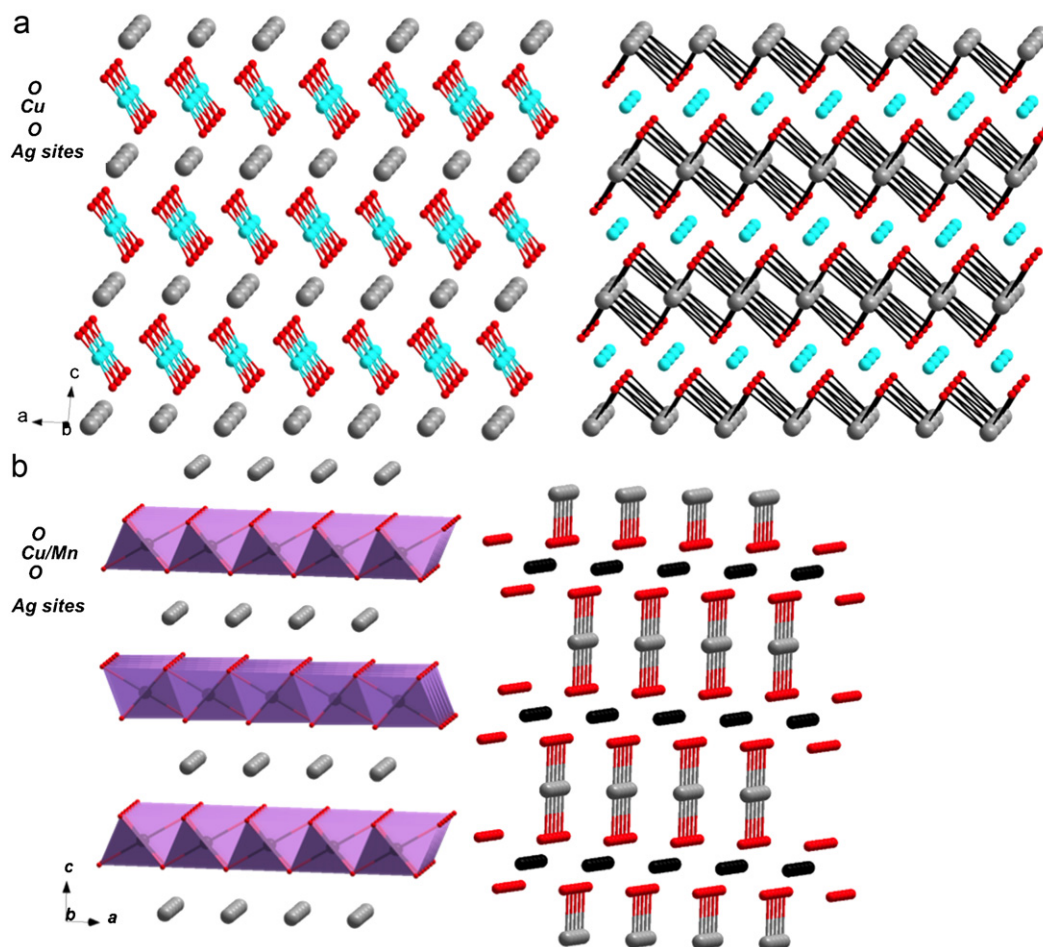


Fig. 1. Structural representation along the (ac) plane of: (a) AgCuO_2 and (b) $\text{AgCu}_{0.5}\text{Mn}_{0.5}\text{O}_2$.

and Mn^{IV} occupy octahedral *B*-sites without evidence of ordering from neutron and electron diffraction. Because of the 3R polytype, the alternate $[\text{AgO}_2]-[(\text{Cu}-\text{Mn})\text{O}_6]$ stacking along [001] exhibits $AbC'CaBb'BcAa'$ sequence with *A*, *B*, *C* standing for the oxygen positions; *a*, *b*, *c* corresponding to the $\text{Cu}^{\text{II}}/\text{Mn}^{\text{IV}}$ cation positions and *a'*, *b'*, *c'* those of Ag^+ . The two dimensional (110) $[(\text{Cu}-\text{Mn})\text{O}_6]_{\infty}$ layers restrict for the conduction of silver between these planes. The synthesis yields pure phase with lattice cell parameters refined of $a = 2.9927(1)\text{\AA}$, $c = 18.431(6)\text{\AA}$ (Fig. 2b). A large particle size distribution from 50 to 500 nm is observed by SEM with the onset of inter-particles twinning yielding doughnut-like morphology (Fig. 2b in inset).

3.2. Transport properties of AgCuO_2 and $\text{AgCu}_{0.5}\text{Mn}_{0.5}\text{O}_2$

The conductivity of AgCuO_2 and $\text{AgCu}_{0.5}\text{Mn}_{0.5}\text{O}_2$ was investigated by four probe DC measurements. Although these phases are air stable, they do not display high thermal stability which prevents any prior sintering process to efficiently improve pellet compactness over 65% (i.e. decomposition from 250 to 300 °C under air). For this reason, even though correction from porosity was considered, it is reasonable to assume that the conductivity values reported are under-estimated. The (*I*-*V*) curves recorded show a linear response (inset in Fig. 3) which attests to the good ohmic contact as well as the good electrochemical stability of the materials. Interestingly, the resistivity of AgCuO_2 and $\text{AgCu}_{0.5}\text{Mn}_{0.5}\text{O}_2$ are different by three orders of

magnitude with resistance values of c.a. 24.4 and 75836 Ω for AgCuO_2 and $\text{AgCu}_{0.5}\text{Mn}_{0.5}\text{O}_2$, respectively, or an electronic conductivity of $3.2 \times 10^{-1} \text{ S/cm}$ for AgCuO_2 and $1.8 \times 10^{-4} \text{ S/cm}$ for $\text{AgCu}_{0.5}\text{Mn}_{0.5}\text{O}_2$. Thermopower measurements demonstrate that electrical conductivity is hole-type with positive Seebeck coefficient of $Q = +2.46$ and $+78.83 \mu\text{V/K}$ for AgCuO_2 and $\text{AgCu}_{0.5}\text{Mn}_{0.5}\text{O}_2$, respectively (Fig. 3). These values clearly reflect a higher charge carrier density in AgCuO_2 .

In the case of $\text{AgCu}_{0.5}\text{Mn}_{0.5}\text{O}_2$, the mixed valence in the *B*-layer (divalent and tetravalent cations) strongly modifies the optical band gap compared to the series. Indeed, while delafossite AgMO_2 (*M* = Al, Sc, Ga, In) member of this series ranges from white to bright orange in color depending on the trivalent cation [11], $\text{AgCu}_{0.5}\text{Mn}_{0.5}\text{O}_2$ powder is dark-brown. This *B*-site modification did not greatly impact the electronic conductivity in comparison with the other AgMO_2 delafossite [11,37–40], reflecting a carrier (hole) trapping effect within the octahedral layers and low mobility, as evidenced the low value determined for $\mu = 1.18 \times 10^{-7} \text{ cm}^2/(\text{Vs})$ at 298 K.

In a similar fashion, the optical band gap of AgCuO_2 is low enough to render the material black. The high p-type conductivity combined to the low Seebeck coefficient suggests that the electronic structure of AgCuO_2 could not be adequately described as $\text{Ag}^+\text{Cu}^{\text{III}}\text{O}_2$ [35,41] by analogy with the closely related NaCuO_2 [6]. This high conductivity and low Seebeck coefficient is accounted by an electronic delocalized state driven by the $4d \langle \text{Ag} \rangle - \sigma^*(\text{Cu}-\text{O})$ orbitals overlapping in agreement with the conclusion drawn by Muñoz-Rojas et al., on the basis of XPS and

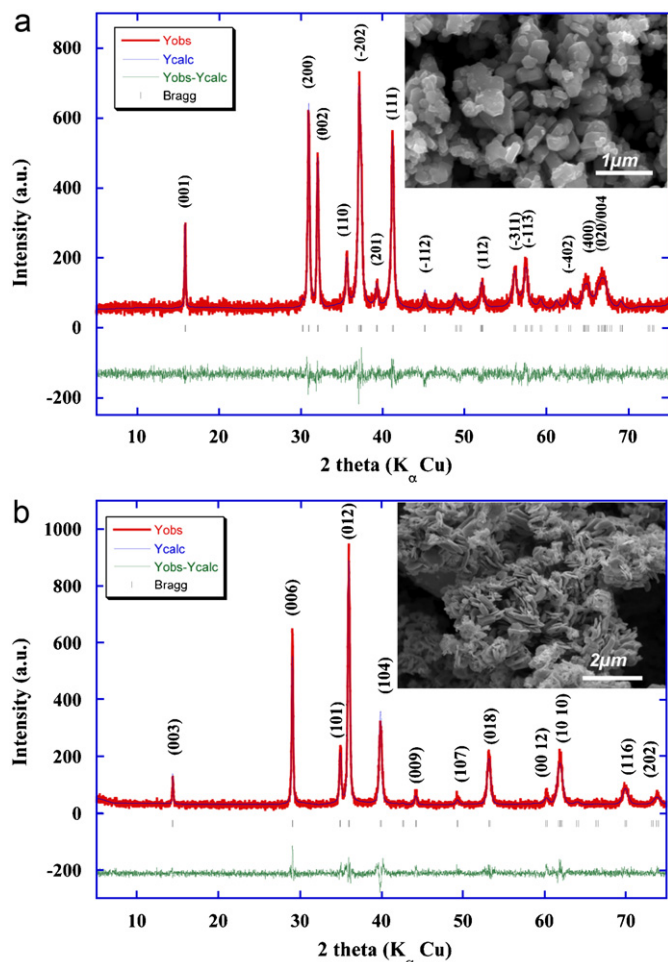


Fig. 2. Full pattern matching refinement of the X-ray diffraction pattern of: (a) AgCuO_2 and (b) $\text{AgCu}_{0.5}\text{Mn}_{0.5}\text{O}_2$. Scanning electron microscopy pictures of the particles in inset.

XANES/EXAFS investigations, who reported the existence of oxidation states higher than +1 and lower than +3 within Ag and Cu sites, respectively [36]. Therefore, the silver in AgCuO_2 is more oxidized which may also explain the enhanced air stability of AgCuO_2 whereas the localized trivalent copper LiCuO_2 , NaCuO_2 and KCuO_2 are all water sensitive [8,42–44].

3.3. Electrochemical properties of AgCuO_2 and $\text{AgCu}_{0.5}\text{Mn}_{0.5}\text{O}_2$ vs. lithium

The ability of these structures to reversibly host lithium ion has been investigated in galvanostatic mode using a current condition equivalent to a C/10 cycling rate (i.e. 1Li^+ inserted or de-inserted in 10 h). The electrochemical-driven lithium insertion into AgCuO_2 proceeds through two distinctive steps. The first, between $x = 0$ and 0.8Li^+ inserted, depicts a monotonous potential-composition decrease corresponding to a solid solution process (Fig. 4). Further in reduction, a potential-composition plateau is observed up to $x = 2\text{Li}^+$ at a 1.5 V (vs. Li^+/Li) cutoff potential. The insertion of 2Li^+ per formula unit confers to AgCuO_2 a gravimetric capacity of 265 mAh/g. The lithium uptake by recharging the cell proceeds with irreversible features. From the very first cycles, only 165 mAh/g is recovered before the reversible capacity fades. The material recharge from $\text{Li}_2\text{AgCuO}_2$ drafts more or less two phenomena situated at 2.6 and 3.1 V (vs. Li^+/Li). At the end of recharge, it is interesting to notice the electrode

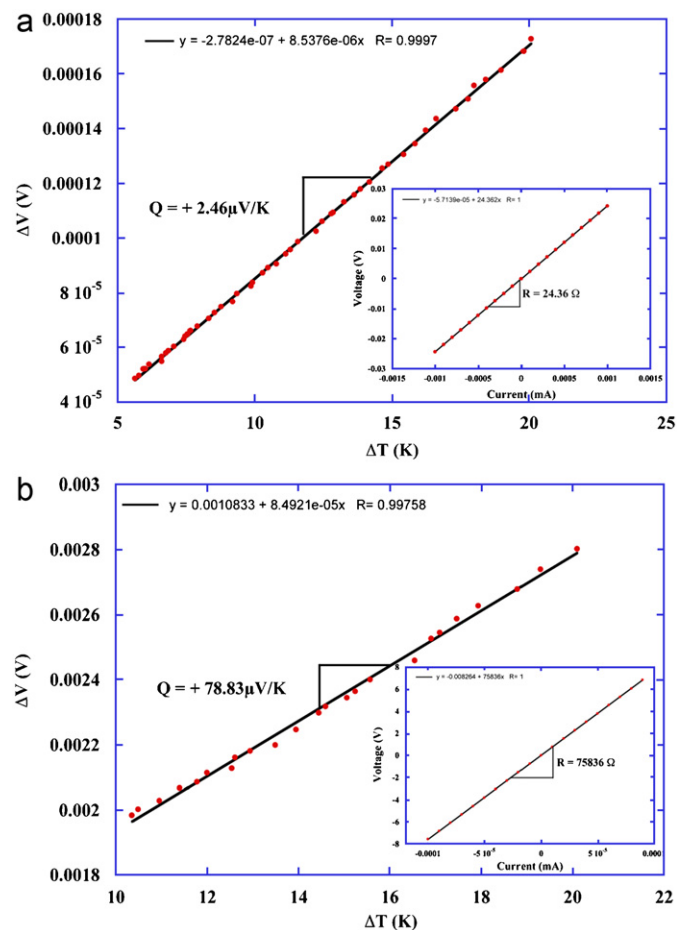


Fig. 3. Thermopower measurements $\Delta T = f(\Delta V)$ for: (a) AgCuO_2 and (b) $\text{AgCu}_{0.5}\text{Mn}_{0.5}\text{O}_2$. Four probes DC conductivity measurements performed at room temperature in inset.

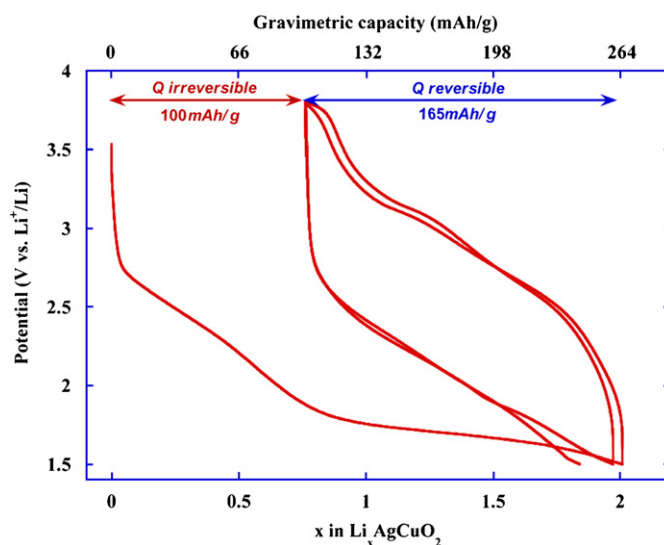


Fig. 4. Two first cycle galvanostatic curve recorded between 1.5 and 3.8 V (vs. Li^+/Li) at C/10 rate for a composite $\text{AgCuO}_2/\text{C}_{sp}$ electrode in 1 M LiPF_6 EC/DMC 1:1 electrolyte.

composition of $\text{Li}_{-0.8}\text{AgCuO}_2$ which corresponds with the composition threshold separating the first and the second discharge phenomenon. The noticeable lower particle size is most likely at

the origin of the better defined discharge trace as compared to Ref. [45], albeit the recovered capacity remains comparable. It is noteworthy the very similar discharge trace between the first solid solution domain and the second discharge. This similitude points out a comparable lithium insertion mechanism involved during initial reduction of AgCuO_2 and in $\text{Li}_{\sim 0.8}\text{AgCuO}_2$. Interestingly, the material discharge proceeds differently in alkaline media. In aqueous electrolyte, the reduction of AgCuO_2 encompasses different phase transition that involves the subsequent formation of $\text{Ag}_2\text{Cu}_2\text{O}_3$, $\text{Ag}^0 + \text{CuO}$, $\text{Ag}^0 + \text{Cu}_2\text{O}$ and then finally at the discharge end $\text{Ag}^0 + \text{Cu}^0$ [9,46]. AgCuO_2 reveals to be a serious cathode candidate for alkaline primary battery since it displays

higher capacity than EMD while maintaining high discharge rate capability [47].

To scrutinize the discrepancy in the reactivity vs. lithium and to prospect whether new Li–Ag–Cu phases could be formed, in situ XRD measurements during the cathode discharge were performed using a D/20 rate (i.e. 1 lithium inserted in 20 h). Fig. 5 shows by different representations the evolution of AgCuO_2 structure between $x = 0$ and 2Li^+ . During the reduction of the material (i.e. lithium insertion), formation of $\text{Ag}_2\text{Cu}_2\text{O}_3$ is never observed, neither CuO nor new defined phases. The lithium insertion induces a rapid decrease in XRD peak intensities, which suggests a structure collapse concomitant with a slight shift in XRD peak that confirms the initial solid solution mechanism (Fig. 5c). Conversely to the $(hk0)$ planes, which are not significantly modified during the discharge, the $[001]$ direction of the structure, which corresponds to the stacking between the dense silver sheets with the CuO_2 layers, is more noticeably affected. This suggests that lithium ions are most likely inserted between these alternating planes inducing very weak $[001]$ contraction. The structure becomes entirely XRD amorphous at a composition of around $x = 0.7\text{--}0.8\text{Li}^+$. This structural collapse most likely results from the difficulties of the structure to accommodate lithium ion owing to the high rigidity of the $[\text{CuO}_4]\text{--}[\text{AgO}_6]$ alternated layers. Whether pure coincidental or not, it is worth pointing out that this threshold composition equals the length of the prior solid solution domain which corresponds remarkably to the extra valence of around 0.7 electron held by the silver as deduced from XPS in ref. [11] (i.e. $\text{Ag}^{+1.7}\text{Cu}^{+2.3}\text{O}_2$ formal oxidation state).

The subsequent plateau recorded at 1.7–1.8 V (vs. Li^+/Li) is attributed to a Li^+/Ag^+ displacement reaction in light of the gradual onset of two very broad diffraction peaks ascribed to silver metal. However, the crossing composition from where the silver reduction is initiated is complex to be accurately determined from XRD because of the nano-crystallinity of the metal withdrawn. It is noteworthy the low reduction potential of silver ion in comparison with 3.45 V for SVOF [18], 3.35 V for SMOF [24], 3.25 V for SVO [48–50] or nearby 3 V for α and β - AgVO_3 [51].

To better understand $(\text{Ag}^0\text{--Li}_2\text{CuO}_2)$ delithiation, a recharged battery cycled one time between 1.5 and 3.80 V (vs. Li^+/Li) was dismantled and the recovered cathode analyzed by XRD. As a result, we experienced the persistence of silver metal diffraction peaks and the X-ray amorphous state of the structure remained. This result indicates that the silver metal is not significantly re-injected inside the structure during the cathode recharge.

From a mechanistic point of view, these results suggest that electron injection into the conduction band of AgCuO_2 during the lithium insertion gradually relieves the mixed valence state hold by the silver and copper. It is therefore expected that the material would be sustaining a metal/insulator transition early during discharge. Such kind of strong band structure modification driven by lithium insertion or de-insertion has ever been experienced throughout multiple examples like for instance in the layered LiCoO_2 [52,53] or by inserting lithium in the hematite $\alpha\text{-Fe}_2\text{O}_3$ [53] or anatase TiO_2 [54]. The insertion of lithium into AgCuO_2 would then result in a drop of the charge carrier concentration near the Fermi level and charges localization while: (i) the silver sites would act as electron acceptor to afford the displacement reaction and (ii) the copper would hold formal oxidation state +III and become gradually reduced to +II in the solid solution domain as schematically summarized below:

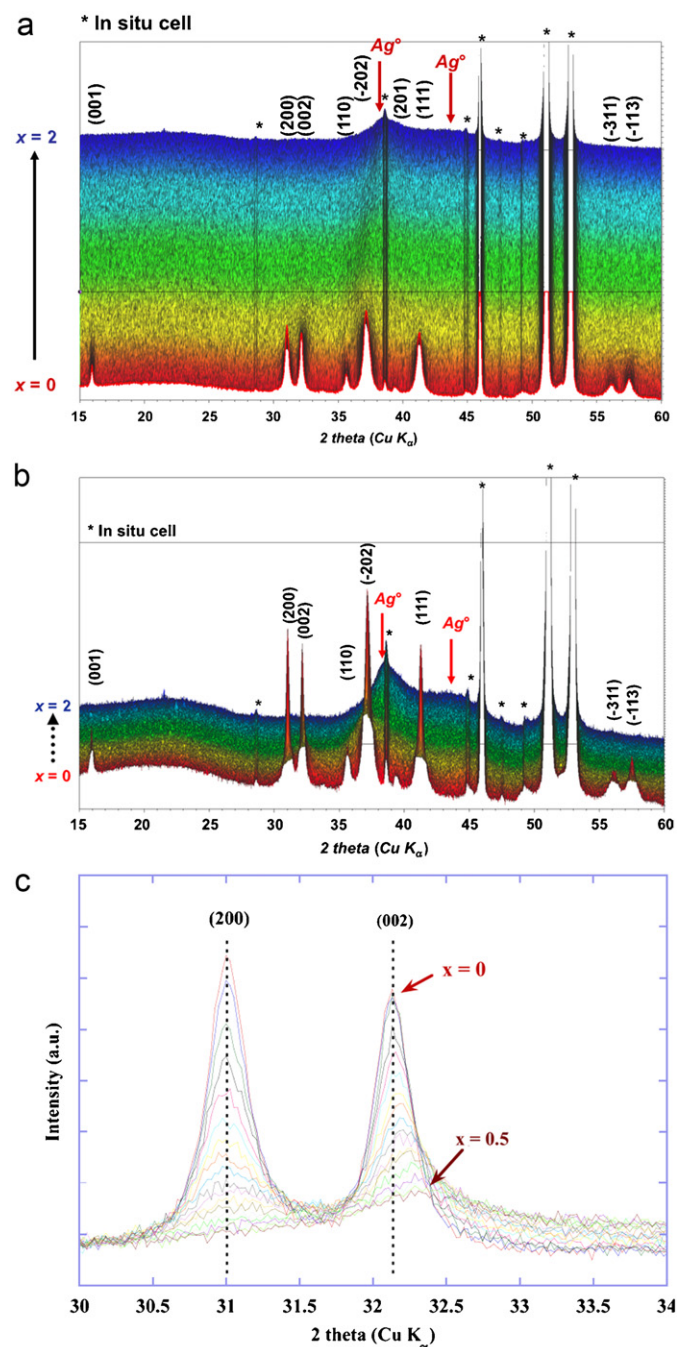
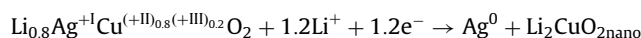
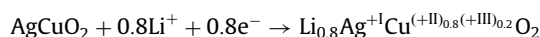


Fig. 5. (a and b) In situ evolution of the XRD pattern recorded during lithium insertion from $\text{Li}_0\text{AgCuO}_2$ and $\text{Li}_2\text{AgCuO}_2$ at C/20 rate in a 2θ range of 15–60° and (c) zoom in the 30–34° diffraction angles between $\text{Li}_0\text{AgCuO}_2$ and $\text{Li}_{0.5}\text{AgCuO}_2$.

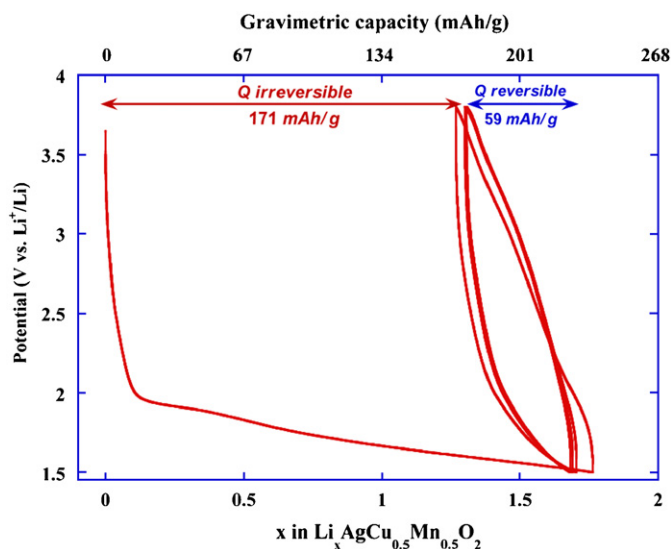


Fig. 6. First cycles galvanostatic curve recorded between 1.5 and 3.8 V (vs. Li^+/Li) at C/10 rate for a composite $\text{AgCu}_{0.5}\text{Mn}_{0.5}\text{O}_2/\text{C}_{\text{sp}}$ electrode in 1 M LiPF_6 EC/DMC 1:1 electrolyte.

This rationalization allows justifying the displacement reaction instead of a classical insertion-type mechanism with the electron injected delocalized within the structure. DFT calculations are actually underway to confirm this scheme and to predict the threshold lithium composition from which the material conduction becomes small polaron-type as well as to evaluate the thermodynamic potential reduction of the silver within AgCuO_2 .

The very few reversible capacity recorded, which involve the reaction of around $1.2\text{Li}^+/\text{e}^-$ per formula unit from $x = 2$ to 0.8, mainly arises from the lithium insertion/de-insertion in/from $\text{LiCu}^{\text{III}}\text{O}_2\text{--Li}_2\text{Cu}^{\text{II}}\text{O}_2$ in a nano-crystalline or an amorphous state (i.e. that can be simplistically schemed as $(\text{Ag}^0\text{--Li}_2\text{CuO}_2)_{\text{nano}} \rightarrow (0.8\text{Ag}^0\text{--Ag}_{0.2}\text{Li}_{0.8}\text{CuO}_2)_{\text{nano}} + 1.2\text{Li}^+ + 1.2\text{e}^-$). The comparable discharge trace between the first and the second discharge could suggest that the aforementioned metal/insulator transition would take place in the very preliminary stage of reduction. The recorded $\text{LiCuO}_2\text{--Li}_2\text{CuO}_2$ signature with the onset of the two phenomena in oxidation is rather comparable with the signature reported by Prakash et al. in crystalline $\text{LiCuO}_2/\text{Li}_2\text{CuO}_2$ [8].

Interestingly, the electrochemical discharge of $\text{AgCu}_{0.5}\text{Mn}_{0.5}\text{O}_2$ has similarities throughout the 1e^- length plateau which takes place in the same potential range as for AgCuO_2 (Fig. 6). $\text{AgCu}_{0.5}\text{Mn}_{0.5}\text{O}_2$ displays a lower capacity above 1.5 V (vs. Li^+/Li) (c.a. 230 mAh/g). The main difference arises from the first portion of the discharge with a much restricted solid solution domain (only $x = 0.1\text{Li}^+$). The cell recharge presents highly irreversible features since solely 0.44 lithium is de-inserted from $\text{Li}_{1.7}\text{AgCu}_{0.5}\text{Mn}_{0.5}\text{O}_2$ (c.a. 59 mAh/g). In situ XRD study during $\text{AgCu}_{0.5}\text{Mn}_{0.5}\text{O}_2$ discharge show in some extent very similar features as for AgCuO_2 with gradual material amorphization coming with the onset of a very broad diffraction peak ascribed to the (111) reflection of silver metal and no new defined compound electrochemically formed during lithium insertion (Fig. 7a). However, conversely to AgCuO_2 , $\text{AgCu}_{0.5}\text{Mn}_{0.5}\text{O}_2$ is still partially XRD crystallized at 1.5 V (vs. Li^+/Li) and no diffraction peak shift is observed like for instance on (006) direction (Fig. 7b). Again because of the nano-crystallinity of the silver withdrawn, it is also difficult here to spot the exact threshold composition from where silver ion starts to be reduced. Therefore, the discharge undergoes

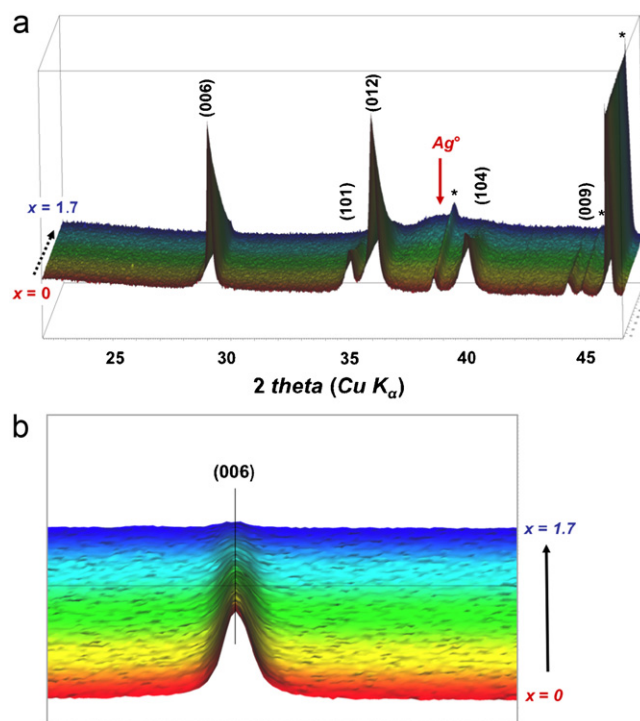


Fig. 7. (a) In situ evolution of the XRD pattern recorded during lithium insertion from $\text{Li}_0\text{AgCu}_{0.5}\text{Mn}_{0.5}\text{O}_2$ and $\text{Li}_{1.7}\text{AgCu}_{0.5}\text{Mn}_{0.5}\text{O}_2$ at C/20 rate in a 2θ range of $22\text{--}47^\circ$ and (b) zoom in the (006) direction.

the reduction of the Mn^{IV} competing with Ag^+ to Ag^0 . More in-depth technique like EXAFS should be considered to determine this discharge threshold and also to clearly attribute the origin of the tiny reversibility arising (i.e. which redox center).

The important potential discrepancy of the silver reduction vs. lithium in AgCuO_2 and $\text{AgCu}_{0.5}\text{Mn}_{0.5}\text{O}_2$ is attributed to the low coordination degree adopted by the silver with the oxygen (coordination 2+4 and 2, respectively) in comparison with the aforementioned silver-based cathode materials (from 5 to 7 in $\text{Ag}_4\text{V}_2\text{O}_6\text{F}_2$ [23], 5 in $\text{Ag}_2\text{V}_4\text{O}_{11}$ and 5 to 7 in $\beta\text{-AgVO}_3$ [55]). Therefore, this low coordination of the silver ion reinforces the covalent character of the $4d(\text{Ag})\text{--}\sigma^*(\text{O})$ bonding causing this cathodic shift of the reduction of the silver in the solid.

4. Conclusion

Additional experiments based on four probes DC conductivity and thermopower measurements have increased our understanding on the transport properties of AgCuO_2 and $\text{AgCu}_{0.5}\text{Mn}_{0.5}\text{O}_2$. A p-type semi-conduction has been observed for both materials, while for AgCuO_2 the delocalized electronic state have been assessed. Electrochemical measurements combined with in situ XRD measurements show that these materials exhibit a Li^+/Ag^+ displacement reaction below 2 V (vs. Li^+/Li) competing with the reduction of Cu^{III} for “ $\text{Li}_x\text{AgCuO}_2$ ” and Mn^{IV} for “ $\text{Li}_x\text{AgCu}_{0.5}\text{Mn}_{0.5}\text{O}_2$ ”. However, the lithium insertion in these two materials does not yield to the formation of new phases. The silver extrusion was found to be almost entirely irreversible and the low reductive potential is explained on the basis of the strong covalent character of the silver ions. DFT calculations are underway to obtain the band structure for both materials and also to confirm the subtle metal/insulator transition upon reduction of AgCuO_2 .

Acknowledgments

The authors gratefully acknowledge Prof. J.-M. Tarascon, Dr. Christine Frayret and Dr. Montse Cabanas from the Laboratoire de Réactivité et Chimie du Solide (UMR-CNRS 6007 Amiens, France) for access to in situ XRD facilities and for fruitful discussions and Pr. T.O. Mason from the department of material science at Northwestern University for access to the thermopower facility. This work was supported by the Office of Naval Research (MURI Grant N00014-07-1-0620), the Department of Energy's Office of Science and the Spanish Ministry of Science and Education (PB98-0491, MAT 2002-04529-C03, MAT 2005-07683_C02_01).

References

- [1] H. Takahashi, K. Igawa, K. Arii, Y. Kamihara, M. Hirano, H. Hosono, *Nature, Letters to Editor*, April 2008, pp. 1–3.
- [2] Y. Kamihara, H. Hiramatsu, M. Hirano, R. Kawamura, H. Yanagi, T. Kamiya, H. Hosono, *J. Am. Chem. Soc.* 128 (21) (2006) 10012–10013.
- [3] C.Y. Liang, R.C. Che, H.X. Yang, H.F. Tian, R.J. Xiao, J.B. Lu, R. Li, J.Q. Li, *Supercond. Sci. Technol.* 20 (2007) 687–690.
- [4] T. Watanabe, H. Yanagi, T. Kamiya, Y. Kamihara, H. Hiramatsu, M. Hirano, H. Hosono, *Inorg. Chem.* 46 (19) (2007) 7719–7721.
- [5] X. Zhao, G. Yu, Y.C. Cho, G. Chabot-Couture, N. Barisic, P. Bourges, N. Kaneko, Y. Li, L. Lu, E.M. Motoyama, O.P. Vajk, M. Greven, *Adv. Mater.* 18 (24) (2006) 3243–3247.
- [6] D.J. Singh, *Phys. Rev. B* 49 (3) (1994) 1580–1585.
- [7] H. Arai, S. Okada, Y. Sakurai, J. Yamaki, *Solid State Ionics* 106 (1998) 45–53.
- [8] A.S. Prakash, D. Larcher, M. Morcrette, M.S. Hegde, J.B. Leriche, C. Masquelier, *Chem. Mater.* 17 (2005) 4406–4415.
- [9] [a] D. Muñoz-Rojas, J. Oro, P. Gomez-Romero, J. Fraxedas, N. Casañ-Pastor, *Electrochem. Commun.* 4 (2002) 684–689;
[b] D. Muñoz-Rojas, J. Oro, J. Fraxedas, P. Gómez-Romero, N. Casañ Pastor, *Cryst. Eng.* 5 (2002) 459–467.
- [10] D. Muñoz-Rojas, J. Fraxedas, P. Gomez-Romero, N. Casañ-Pastor, *J. Solid State Chem.* 178 (2005) 295–305.
- [11] W.C. Sheets, E.S. Stampler, M.I. Bertoni, M. Sasaki, T.J. Marks, T.O. Mason, K.R. Poeppelmeier, *Inorg. Chem.* 47 (7) (2008) 2696–2795.
- [12] C. Tubandt, E. Lorenz, *Z. Phys. Chem.* 87 (1914) 513–542.
- [13] H.F. Hsu, S. Loo, F. Guo, W. Chen, J.S. Dyck, C. Uher, T. Hogan, E.K. Polychroniadis, M.G. Kanatzidis, *Science* 303 (2004) 818–820.
- [14] Y.G. Vlasov, E.A. Bychkov, B.L. Seleznev, *Sensors Actuators B* 2 (1990) 23–31.
- [15] K.J. Takeuchi, A.C. Marschilok, S.M. Davis, R.A. Leising, E.S. Takeuchi, *Coord. Chem. Rev.* 219 (2001) 283–310.
- [16] G. Taillades, J. Sarradin, *J. Power Sources* 125 (2004) 199–205.
- [17] R. Kanno, Y. Takeda, T. Ichikawa, K. Nakanishi, O. Yamamoto, *J. Power Sources* 26 (1989) 535–543.
- [18] F. Sauvage, V. Bodenez, H. Vezin, T.A. Albrecht, J.-M. Tarascon, K.R. Poeppelmeier, *Inorg. Chem.* 47 (19) (2008) 8464–8472.
- [19] M. Onoda, K. Kanbe, *J. Phys. Condens. Matter* 13 (2001) 6675–6685.
- [20] R.A. Leising, W.C. Thiebolt III, E.S. Takeuchi, *Inorg. Chem.* 33 (1994) 5733–5740.
- [21] R.P. Ramasamy, C. Feger, T. Strange, B.N. Popov, *J. Appl. Electrochem.* 36 (2006) 487–497.
- [22] J.W. Lee, B.N. Popov, *J. Power Sources* 161 (2006) 565–572.
- [23] E.M. Sorensen, H.K. Izumi, J.T. Vaughey, C.L. Stern, K.R. Poeppelmeier, *J. Am. Chem. Soc.* 127 (17) (2005) 6347–6352.
- [24] W. Tong, G.G. Amatucci, *Electrochem. Soc.* 702 (2007) 278 (Meeting abstract).
- [25] D. Muñoz-Rojas, G. Subias, J. Oro-Solé, J. Fraxedas, B. Martinez, M. Casas-Cabanas, J. Canales-Vazquez, J. Gonzales-Calbet, E. Garcia-Gonzalez, R.I. Walton, N. Casañ-Pastor, *J. Solid State Chem.* 179 (2006) 3883–3892.
- [26] E.M. Tejada-Rosales, M.R. Palacín, P. Gómez-Romero, *Bol. Soc. Esp. Cerám. Vidrio* 39 (3) (2000) 209–212.
- [27] P. Gómez-Romero, E.M. Tejada-Rosales, M.R. Palacín, *Angew. Chem. Int. Ed.* 38 (4) (1999) 524–525.
- [28] E.M. Tejada-Rosales, J. Rodríguez-Carvajal, N. Casañ-Pastor, P. Alemany, E. Ruiz, S. Alvarez, P. Gómez-Romero, *Inorg. Chem.* 41 (2002) 6604–6613.
- [29] J. Rodríguez-Carvajal, *Physica B* 192 (1993) 55–59.
- [30] J. Rodríguez-Carvajal, FullProf Program: Multipattern Rietveld, Profile Matching and Integrated Intensity Refinement of X-ray and Neutron Diffraction Data, Version 1.9c, May 2001—Laboratoire Leon Brillouin, CEA-CNRS, JRC.
- [31] P. Thompson, D.E. Cox, J.B. Hastings, *J. Appl. Crystallogr.* 20 (1987) 79–83.
- [32] D.S. McLachlan, M. Blaszkiewicz, R.E. Newnham, *J. Am. Ceram. Soc.* 73 (8) (1990) 2187–2202.
- [33] H.L. Tuller, A.S. Nowick, *J. Phys. Chem. Solids* 38 (1977) 859–867.
- [34] A.F. Ioffe, *Physics of Semiconductors*, Infosearch, London, 1960.
- [35] J. Curda, W. Klein, H. Liu, M. Jansen, *J. Alloys Compd.* 338 (2002) 99–103.
- [36] D. Muñoz-Rojas, J. Fraxedas, G. Subias, P. Gomez-Romero, N. Casañ-Pastor, *J. Phys. Chem. B* 109 (2005) 6193–6203.
- [37] R.D. Shannon, D.B. Rogers, C.T. Prewitt, J.L. Gillson, *Inorg. Chem.* 10 (1971) 723–727.
- [38] K.A. Vanaja, R.S. Ajimsha, A.S. Asha, M.K. Jayaraj, *Appl. Phys. Lett.* 88 (2006) 212103/1–212103/3.
- [39] T. Otake, K. Ueda, A. Kudoh, H. Ozono, H. Kawazoe, *Appl. Phys. Lett.* 72 (1998) 1036–1038.
- [40] J.E. Clayton, D.P. Cann, N. Ashmore, *Thin Solid Films* 411 (2002) 140–146.
- [41] J. Curda, W. Klein, M. Jansen, *J. Solid State Chem.* 162 (2001) 220–224.
- [42] T.L. Friedman, A.M. Stacy, *J. Solid State Chem.* 109 (1994) 203–204.
- [43] J. Pickardt, W. Paulus, M. Schmalz, R. Schollhorn, *J. Solid State Chem.* 89 (1990) 308–314.
- [44] N.E. Brese, M. O'Keefe, R.B. Von Dreele, V.G. Young, *J. Solid State Chem.* 83 (1989) 1–7.
- [45] C.D. May, J.T. Vaughey, *Electrochem. Commun.* 6 (2004) 1075–1079.
- [46] F. Wang, C. Eylem, K. Nanjundaswamy, N. Iltchev, *Electrochem. Solid State Lett.* 7 (10) (2004) A346–A347.
- [47] T.W. Jones, J.S. Forrester, A. Hamilton, M.G. Rose, S.W. Donne, *J. Power Sources* 172 (2007) 962–969.
- [48] R.A. Leising, W.C. Thiebolt III, E.S. Takeuchi, *Inorg. Chem.* 33 (1994) 5733–5740.
- [49] K. West, A.M. Crespi, *J. Power Sources* 54 (1995) 334–337.
- [50] N.D. Leifer, A. Colon, K. Martocci, S.G. Greenbaum, F.M. Alamgir, T.B. Reddy, N.R. Gleason, R.A. Leising, E.S. Takeuchi, *J. Electrochem. Soc.* 154 (6) (2007) A500–A506.
- [51] S. Zhang, W. Li, C. Li, J. Chen, *J. Phys. Chem. B* 110 (2006) 24855–24863.
- [52] S. Levasseur, M. Ménétrier, E. Suard, C. Delmas, *Solid State Ionics* 128 (2000) 11–24.
- [53] F. Sauvage, J.-M. Tarascon, E. Baudrin, *J. Phys. Chem. C* 111 (26) (2007) 9624–9630.
- [54] R. Van de Krol, A. Goossens, E.A. Meulenkaamp, *J. Appl. Phys.* 90 (5) (2001) 2235–2242.
- [55] P. Rozier, J.-M. Savariault, J. Galy, *J. Solid State Chem.* 122 (1996) 303–308.